Strong-field effects of the one-dimensional hydrogen atom in momentum space

Ue-Li Pen* and T. F. Jiang
Department of Electrophysics, National Chiao Tung University, Hsinchu 30050, Taiwan, Republic of China
(Received 3 April 1992)

The time evolution of the ground state of a one-dimensional hydrogen atom in the intense laser pulse is studied directly in momentum space. A finite matrix representation of operators is developed to solve nonperturbatively the time-dependent Schrödinger equation. We find that some numerical limitations in coordinate space of above-threshold ionization (ATI) can be overcome, and clear physical interpretations of the numerical data are possible. Both the ATI and harmonic-generation spectra are obtained. The correlations between these two multiphoton phenomena are discussed.

PACS number(s): 32.80.Rm, 32.90.+a

I. INTRODUCTION

Since the experimental report of above-threshold-ionization (ATI) phenomena [1], the study of the behavior of atoms under the irradiation of strong laser fields has been a subject of intensive interest [2]. When the laser-atom interaction term is comparable to nuclear Coulombic attraction, the quantum-mechanical perturbation method is no longer valid in the calculation of multiphoton processes, and nonperturbative techniques are then required. The problem of a real atom subjected to strong laser fields is difficult, even for the case of a one-electron atom [3]. A number of one-dimensional model potentials have been employed to explore some insights into the problem [4]. In many previous numerical works, the coordinate space grids were usually adopted to investigate the multiphoton dynamics. Intuitively, when the atomic electron is driven to ionize, its wave function becomes spatially widely spread. Therefore the calculation in coordinate space requires either a large number of grid points or a considerable size of basis set functions to simulate the event. Though sometimes a filter function can be put near the grid boundary to model the ionization mechanism and to avoid wave reflection from the boundary [5], some dynamics of the ionized electron is inevitably lost by filtering. However, the spreading of a wave function in coordinate space does not necessarily imply the spreading in the momentum space (p space). In fact, the observed narrow ATI peaks in electron energies suggest that the wave functions are highly localized in p space and encourage such studies. For current super-intense experimental laser sources, the atomic electron can absorb several to several dozen photons before and after ionization. The change in electron momentum is mainly due to the absorption of photons. The spreading of the photoelectron in p space is far more limited. It would thus be instructive to study the problem in p space directly. Motivated by this concept, we believe the p-space approach to be of practical value. This approach is generally not easy to implement on the differential-type Schrödinger equation [6].

In this paper we present an alternative approach which resolves most of the aforementioned difficulties. We approximate the observable by a finite-dimensional matrix operator in p space. Then we proceed to solve the time-dependent Schrödinger equation in matrix form. Since matrix operations are fully vectorizable, the calculation is very efficient on a vector or parallel machine. We find that both the bound-continuum and continuum-continuum dipole transition matrix elements are straightforward to calculate. These matrix elements play important roles in multiphoton processes. The spectra of ATI and harmonic generation are obtained from the *same* calculation. And the correlation between these two multiphoton processes is explored. This point has rarely been mentioned in previous calculations. By examining the p-space wavefunction, we also gain considerable insight into the nature of the ATI processes.

We describe our approach in the Sec. II. The results of the one-dimensional hydrogen-atom ATI and harmonic generation will be presented in Sec. III. This is followed by a conclusion and suggestions for further investigations in Sec. IV. Atomic units are used throughout.

II. MOMENTUM-SPACE MATRIX APPROACH FORMULATION

A. Model atom

Although recently a softened Coulomb potential has been popular for studying the strong field problem [4], we prefer the basic Coulomb potential model in our study

$$\hat{H}_0 = \frac{\hat{p}^2}{2} + \begin{cases} -1/x & \text{if } x > 0 \\ \infty & \text{if } x \le 0. \end{cases} \tag{1}$$

This model offers the following appealing features.

(i) The one-dimensional Schrödinger equation corresponding to Eq. (1) is closely related to the s-state radial equation of a real hydrogen atom. If we write the eigenfunction of the three-dimensional hydrogen atom as

$$\Psi_{nlm}(r,\theta,\phi) = Y_{lm}(\theta,\phi)\chi_{nl}(r)/r, \tag{2}$$

then χ satisfies the following equation:

$$-\frac{1}{2}\frac{\partial^2\chi}{\partial r^2}+\left(-\frac{1}{r}+\frac{l(l+1)}{r^2}\right)\chi=E\chi. \tag{3}$$

It reduces to Eq. (1) as $l \to 0$ and its properties have been thoroughly studied [7].

(ii) The model atom has been used successfully in the study of microwave ionization of Rydberg hydrogen atoms [8] and surface-state electrons in liquid helium [9]. It has proved itself to be a good model in those cases. The extension of the one-dimensional hydrogenic model to strong field problems of current interest appears worthwhile.

(iii) As we will show below, the Coulomb singularity at the origin of coordinate space causes no difficulties in our p-space approach.

(iv) The wave function χ_{nl} in Eq. (3) vanishes at $r=0$. By symmetry, the p-space projection of this wave function must be an odd function, so that we only need to consider the positive momentum components. This reduces the numerical effort significantly.

B. Finite matrix representation

Following Dirac [10], for the observable $\hat{x}$ we have

$$\hat{x}\cdot\hat{x}=\hat{x}^2, \tag{4}$$

$$\hat{x}\cdot\frac{\hat{1}}{x}=I. \tag{5}$$

An operator corresponding to the observable is represented by an infinite-dimensional matrix. But in practical calculations, since the space we work with is only finite dimensional, the identity equation (5) does not hold manifestly:

$$\sum_{j=1}^{n}(x)_{ij}\left(\frac{1}{x}\right)_{jk}=\sum_{j=1}^{n}\langle i|x|j\rangle\left\langle j\left|\frac{1}{x}\right|k\right\rangle \tag{6}$$

$$=\delta_{ik}-\sum_{j=n+1}^{\infty}\langle i|x|j\rangle\left\langle j\left|\frac{1}{x}\right|k\right\rangle. \tag{7}$$

To be consistent with $\hat{x}\cdot\hat{1}/x=I$ in real calculations, we make the following ansatz [11]:

$$\sum_{j=1}^{n}(x)_{ij}\left(\frac{1}{x}\right)_{jk}=\delta_{ik}. \tag{8}$$

With this understanding, it becomes straightforward to compute matrix representations for various functionals of $\hat{x}$, once we define *one* representation thereof. For example, if we diagonalize $\hat{x}$ into its eigenvalue matrix Λ_x by

$$S^\dagger\hat{x}S=\Lambda_x, \tag{9}$$

then

$$S^\dagger\hat{x}SS^\dagger\frac{\hat{1}}{x}S=I \tag{10}$$

gives

$$\left(\frac{\hat{1}}{x}\right)=S\Lambda_x^{-1}S^\dagger. \tag{11}$$

C. Momentum-space method

The wave function ψ in momentum space is an n vector representing the sampling of the projection $\langle p|\psi\rangle$. Observables are expressed as matrix operators on the vectors. The momentum operator $\hat{p}$ is clearly a diagonal matrix

$$\hat{p}_{ij}=j\triangle p\ \delta_{ij}, \tag{12}$$

where $\triangle p=p_{\max}/N$ is determined from the maximum momentum $p_{\max}$ and number of grid points N in the calculation. The operator $\hat{x}^2$ is approximated by the second-order derivative

$$\hat{x}^2_{ij}=\frac{-1}{\triangle p^2}(\delta_{i,j+1}-2\delta_{ij}+\delta_{i,j-1}). \tag{13}$$

The eigenfunctions ϕ_j and eigenvalues λ_k of this matrix are analytically known to be [12]

$$\lambda_k=\frac{4}{\triangle p^2}\sin^2\frac{\pi k}{2N},\qquad k=1,2,\ldots,N-1 \tag{14}$$

$$\phi_j^{(k)}=\sin\frac{\pi jk}{N},\qquad j=1,2,\ldots,N-1. \tag{15}$$

Now we can calculate any dynamical variable which is a function of $\hat{x}$. For example, the matrix elements of $\hat{x}^2$ are in factored form:

$$(x^2)_{ij}=\sum_{k=1}^{N}\lambda_k\phi_i^{(k)}\phi_j^{(k)}. \tag{16}$$

The choice of defining everything from a second derivative in Eq. (13) arises from the necessity of having only positive eigenvalues, which, as we argued earlier, will reduce the required calculations.

We can then find the p-space finite-matrix representation of $\hat{x}$ and $\hat{1}/x$ by the way described in Sec. II B. In our calculation, we use a maximum momentum value $p_{\max}=5.0$ and N (number of grid points)$=1000$. Diagonalization of H_0 in p space gives 24 bound states and 976 discretized pseudocontinuum states. The accuracy of the lowest five energy levels is within 1–3 %. To check the applicability of the discrete p-space computations for time-dependent behavior, we calculate the transition dipole matrix elements for bound-continuum and continuum-continuum transitions. These matrix elements are important to multiphoton processes. Susskind and Jensen [13] developed a p-space Sturmian basis method to obtain the relevant matrix elements. The calculation presented here is much simpler than theirs from the viewpoint of numerical treatment.

1. Bound-continuum dipole matrix elements

The dipole matrix elements from bound state $|n\rangle$ to continuum state $|p\rangle$ are analytically known [13]. Numerically, since

$$[\hat{x},\hat{H}_0]=i\hat{p}, \tag{17}$$

$$\langle n|[\hat{x},\hat{H}_0]|p\rangle=i\langle n|\hat{p}|p\rangle, \tag{18}$$

we obtain

$$x_{n,p} = \frac{i}{\varepsilon_p - E_n}\langle n|\hat{p}|p\rangle. \tag{19}$$

We calculate the eigenfunctions $|n\rangle$ and $|p\rangle$ directly from the diagonalization of H_0, and ε_p, E_n are the corresponding eigenenergies of states $|p\rangle$ and $|n\rangle$, respectively. In Fig. 1(a) the calculated dipole matrix elements of $|n = 1\rangle$ to continuum states in the momentum range $p = 0.0$–5.0 are plotted, together with their exact counterpart. The agreement is quite good.

2. *Continuum-continuum dipole matrix elements*

The continuum-continuum matrix elements are calculated numerically exactly in the same way as those of bound-bound, bound-continuum transitions without any extra effort. We plot the matrix elements of continuum states with $p \approx 0.1$ to $p = 0.0$–0.3 in Fig. 1(b). Due to a difference in normalization convention, the magnitude of matrix elements may differ from Ref. [13], but the agreement in the final structure is satisfactory [14].

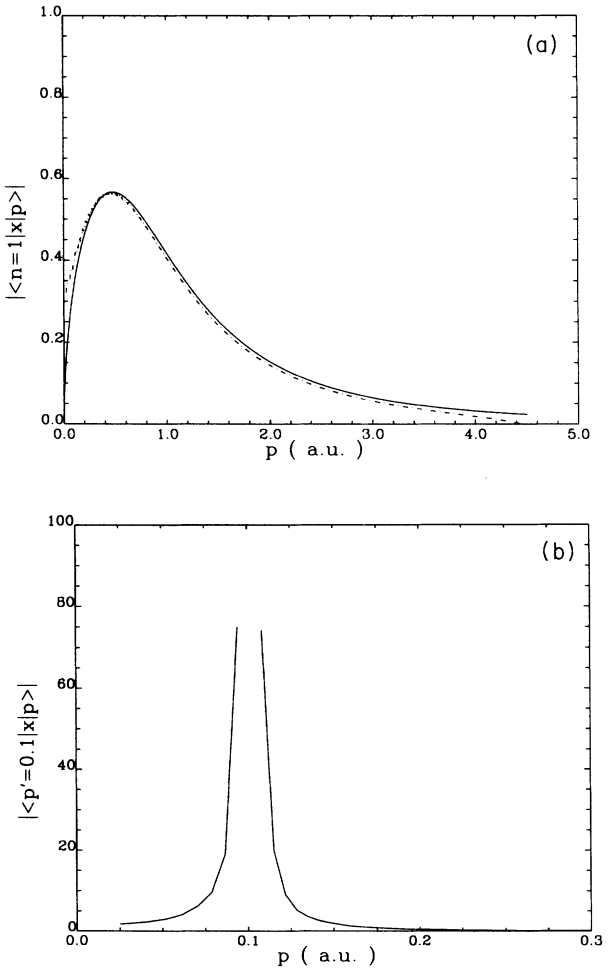

FIG. 1. (a) *Bound-continuum* dipole matrix elements of state $|n = 1\rangle$ to continuum state $|p\rangle$. Solid curve, p-space calculation; dot-dashed curve, analytic results. (b) *Continuum-continuum* dipole matrix elements of state $|p = 0.101\,26\rangle$ to $|p\rangle$, $p = 0$–5.0.

D. Time evolution

We consider the one-dimensional hydrogen atom under the influence of a strong laser pulse. For currently available laser source wavelengths (10^2–10^3nm), the dipole approximation is adequate. We write the time-dependent Schrödinger equation as

$$i\frac{\partial\psi}{\partial t} = \left(\frac{p^2}{2} - \frac{1}{x} + xE(t)\right)\psi, \tag{20}$$

where $E(t)$ is the electric field amplitude of the laser light. We model the electric field as a monochromatic wave adiabatically turned on and off:

$$E(t) = F_m \sin(\omega t)\sin^2\left(\frac{\pi t}{T}\right), \tag{21}$$

where T is the laser pulse duration and ω is the laser frequency. The system is initially prepared in the ground state of H_0, and $\hat{x}$ and $\hat{1}/x$ are in their truncated but self-consistent momentum representation. The time-dependent equation is integrated in momentum space by a Runge-Kutta-Verner fifth- and sixth-order method to the final time T.

III. RESULTS

We calculate in this paper the response of the model atom under the irradiation of laser pulses with wavelength $\lambda = 248$ nm and field strengths $F_m = 0.025$, 0.05, 0.1, and 0.2 a.u. (A peak field of 1 a.u. corresponds to a laser intensity of 3.51×10^{16} W/cm^2). This light source is currently available from the Kr-F laser system [15].

A. ATI

In Figs. 2(a)–2(d), we plot the projection of the evolved wave function $\psi(p, t = 20\tau)$, with τ being the laser period, onto the zero-field unperturbed eigenstates. We define the energy $E_{\text{threshold}}$ as

$$E_{\text{threshold}} = n\hbar\omega + E_0 - \frac{F_m^2}{4\omega^2}, \tag{22}$$

where E_0 is the calculated ground-state energy and n is the smallest integer ensuring $E_{\text{threshold}} > 0$. The last term is the pondermotive shift. An atomic electron oscillates with the rapid driving field at this average energy. The electron absorbs photons to overcome the ionization potential and additionally stores an extra amount of energy to oscillate in the laser region. The pondermotive energy will finally be released if the electron decelerates out of the laser region adiabatically. This effect corresponds to the *long pulse* regime where the laser pulse duration is much longer than the time it takes for the photoelectron to leave the focus region. In Figs. 2(a)–2(d) we see the ATI structure at various field strengths. The number of ATI peaks increases with higher field

strengths. Also the lower-energy primary peaks in both $F_m = 0.025$ and 0.05 a.u. have almost disappeared at $F_m = 0.1$ and 0.2 a.u., mainly due to the shift of threshold energy $E_{\text{threshold}}$. These are features of the well-known *peak switching* and *peak suppression* effects of strong field phenomena.

Recently, Reed and Burnett [4] analyzed the ATI peak structure of a one-dimensional softened Coulomb atom under the same laser profile. The satellite peaks associated with ATI peaks as shown in Fig. 2(c) are interpreted as quantum interference of waves produced at the rising and falling portions of the pulse. The formulas for the positions of the maxima and minima of the satellite peaks are given explicitly. Comparing the peaks from the $4\hbar\omega$ and $5\hbar\omega$ in Fig. 2(c), which have dominant satellite peaks to their results, we obtain quantitative agreement of maxima and minima positions with their formulas.

In Figs. 3(a)–3(d), we show the the time-evolved wave functions at $t = 20\tau$ in p space. The threshold momentum $p_{\text{threshold}}$ is defined as

$$p_{\text{threshold}} = \sqrt{2E_{\text{threshold}}}. \tag{23}$$

The peaks to the right of $p_{\text{threshold}}$ correspond directly to the ATI spectrum. The background level is simply due to the bound states, which have broadband p-space dispersion [16]:

$$|\psi_n(p)|^2 = \frac{2}{\pi}\frac{p_n^3}{(p^2+p_n^2)^2}, \tag{24}$$

where $p_n = \sqrt{-2mE_n}$, and $E_n = -1/2n^2$ is the bound-state energy corresponding to state $|n\rangle$. This is a special feature of the p-space calculation: the lower-energy bound states of the Hamiltonian have a wider p-space spread, with ever decreasing widths as one advances to excited and continuum states. The latter are almost δ functions in p space. If we compare Fig. 2(c) with Fig. 3(c), we notice that the bound peak in Fig. 2(c) (to the left of the dashed line) is a broad spread to the left of the dashed line in Fig. 3(c). The qualitative difference between bound states and continuum states is apparent. We can now *see* states more clearly once they are ionized, which is a definite advantage if we hope to understand processes between continuum states. Similarly, we do not expect to waste excessive resolution on excited bound-state dynamics, and for ATI problems we desire

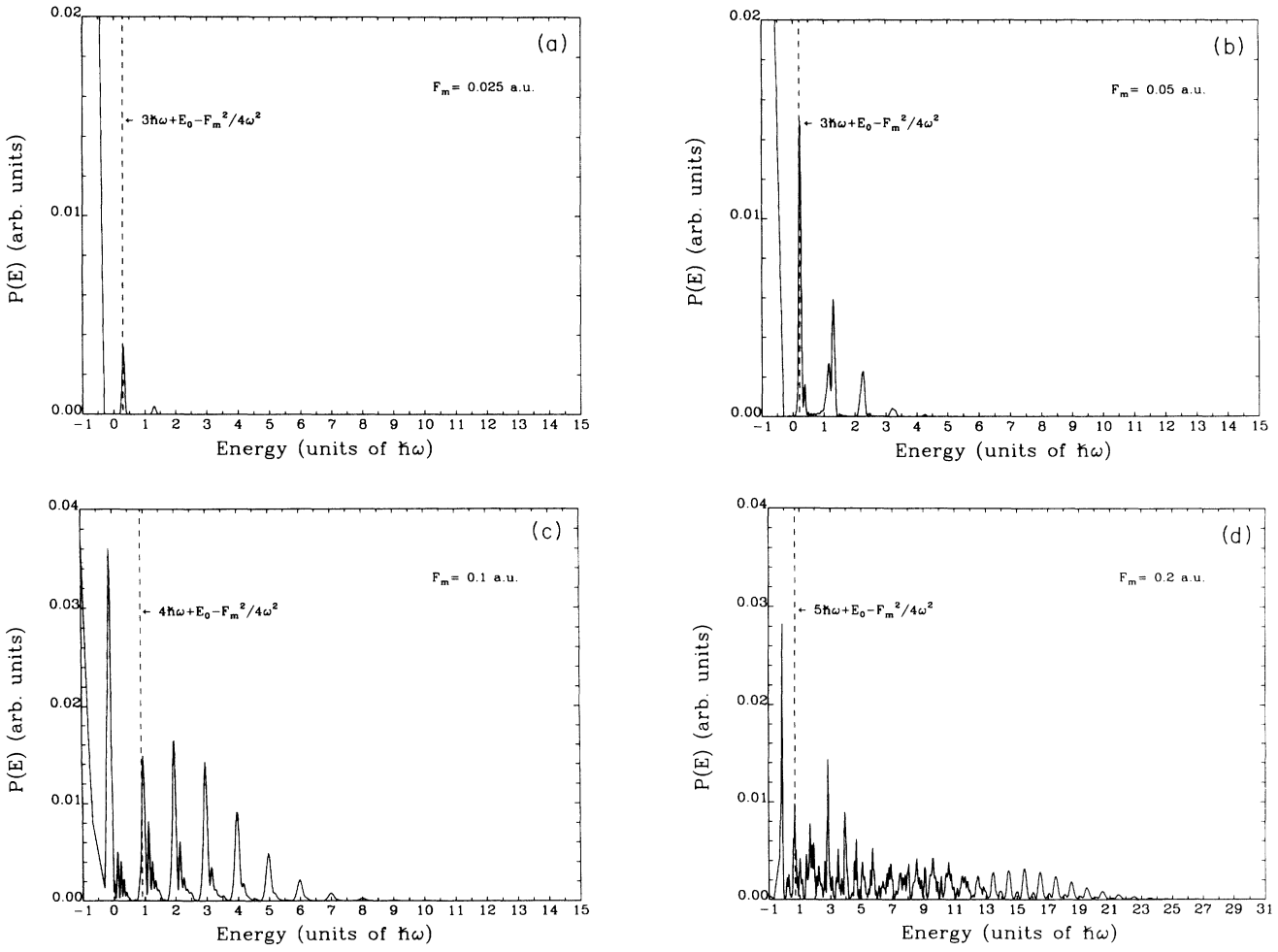

FIG. 2. ATI spectra. Peaks with electron energy to the right of the vertical dashed line are ATI peaks. Negative-energy peaks are due to bound states. (a) $F_m = 0.025$ a.u., (b) $F_m = 0.05$ a.u., (c) $F_m = 0.1$ a.u., (d) $F_m = 0.2$ a.u.

just such a feature in order to model the scenario on a computer without spending time on irrelevant dynamics. In p space none of the coordinate limitations plagues us any more, electrons do not leave the grid, and the resolution becomes neither too large nor too small to resolve the desired effects.

During the calculation, we find that the wave functions at all studied field strengths are localized within $p \leq 5.0$. This shows that the choice of $p_{\max} = 5.0$ is reasonable and confirms the computational advantages of the present p-space approach.

B. Harmonic generation

Recently it was pointed out that for a nonvanishing final dipole moment function, the correct harmonic-generation spectrum must be given from the dipole acceleration function instead of length form itself [17]. In Figs. 4(a)–4(d), we plot the calculated harmonic-generation spectra using the acceleration form. The spectra are obtained through

$$I(\omega) \propto \left| \int_0^T e^{-i\omega t} \langle \ddot{x}(t) \rangle dt \right|^2 . \tag{25}$$

In calculating $\langle \ddot{x}(t) \rangle$ Ehrenfest's theorem is used:

$$\begin{aligned} \langle \ddot{x}(t) \rangle &= \left\langle \psi(t) \middle| -\frac{1}{x^2} - E(t) \middle| \psi(t) \right\rangle \\ &= \left\langle \psi(t) \middle| -\frac{1}{x^2} \middle| \psi(t) \right\rangle - E(t). \end{aligned} \tag{26}$$

The above calculations were carried out in p space. The qualitative picture of harmonic-generation spectrum characteristics [18] is obtained for weak fields. At stronger fields F_m =0.1 and 0.2 a.u., the characteristics are less clear. We have recently carried out a study of

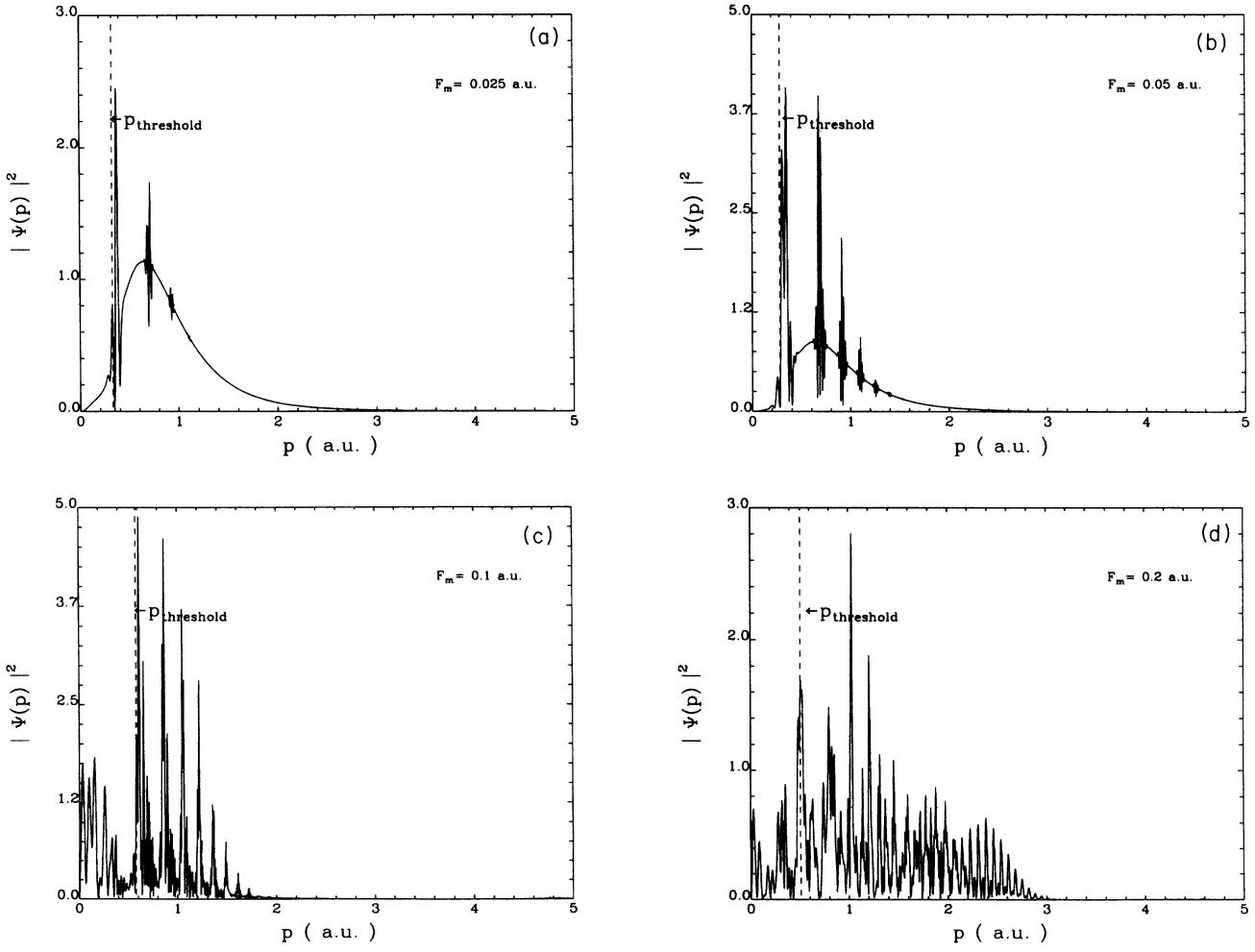

FIG. 3. Wave function after 20 laser periods, i.e., the end of the laser pulse. The features to the right of the vertical dashed line are related to ATI structure. (a) $F_m = 0.025$ a.u., (b) $F_m = 0.05$ a.u., (c) $F_m = 0.1$ a.u., (d) $F_m = 0.2$ a.u.

the harmonic-generation spectrum for a real hydrogen atom. We find that for higher field strength, more angular momentum components need to be included to obtain convergent results. For F_m =0.1 a.u., orbital angular momenta up to $l_{\max}$ = 40 are included in the calculation. And only the odd harmonic orders appear due to parity symmetry [19]. In the present one-dimensional case, there is no parity symmetry. This results in the appearence of even harmonic orders in addition to odd harmonic orders [20].

For comparison, the length form of the dipole function is

$$\langle x(t)\rangle = \langle\psi(t)|x|\psi(t)\rangle. \tag{27}$$

In Fig. 5(a), the variation of $\langle\ddot{x}(t)\rangle$ with respect to time at F_m =0.2 a.u. is shown. Since the driving field has been removed, as shown in Eq. (26), its frequency spectrum gives only the radiation from the **charge** itself. Incorporating the acceleration form, we obtain the results shown in Figs. 4(a)–4(d). Figure 5(b) shows an example of the time change of the length form $\langle x(t)\rangle$. We find that, after 5τ, $\langle x(t)\rangle$ increases rapidly along with a smaller fluctuation at the laser driving frequency. The monotonic part contributes a strong continuous radiation background from bremsstrahlung. The background washes out the harmonic-generation signals, which are relatively weaker. This effect will be increasingly dominant for stronger fields. In Figs. 6(a) and 6(b) we show the harmonic-generation spectra generated from the length form of the dipole function at the lowest and highest field strengths calculated.

Since we have calculated both the ATI and harmonic spectra in this study, it would be interesting to consider the correlation between these two multiphoton phenomena. It was discussed by Eberly, Su, and Javanainen [21] that the two spectra are closely related as long as the initial-state population is dominant during the process. In Fig. 7(a) we plot the survival probability of the ground state as a function of time. We find that, for both F_m =0.025 and F_m =0.05 cases, the ground-state

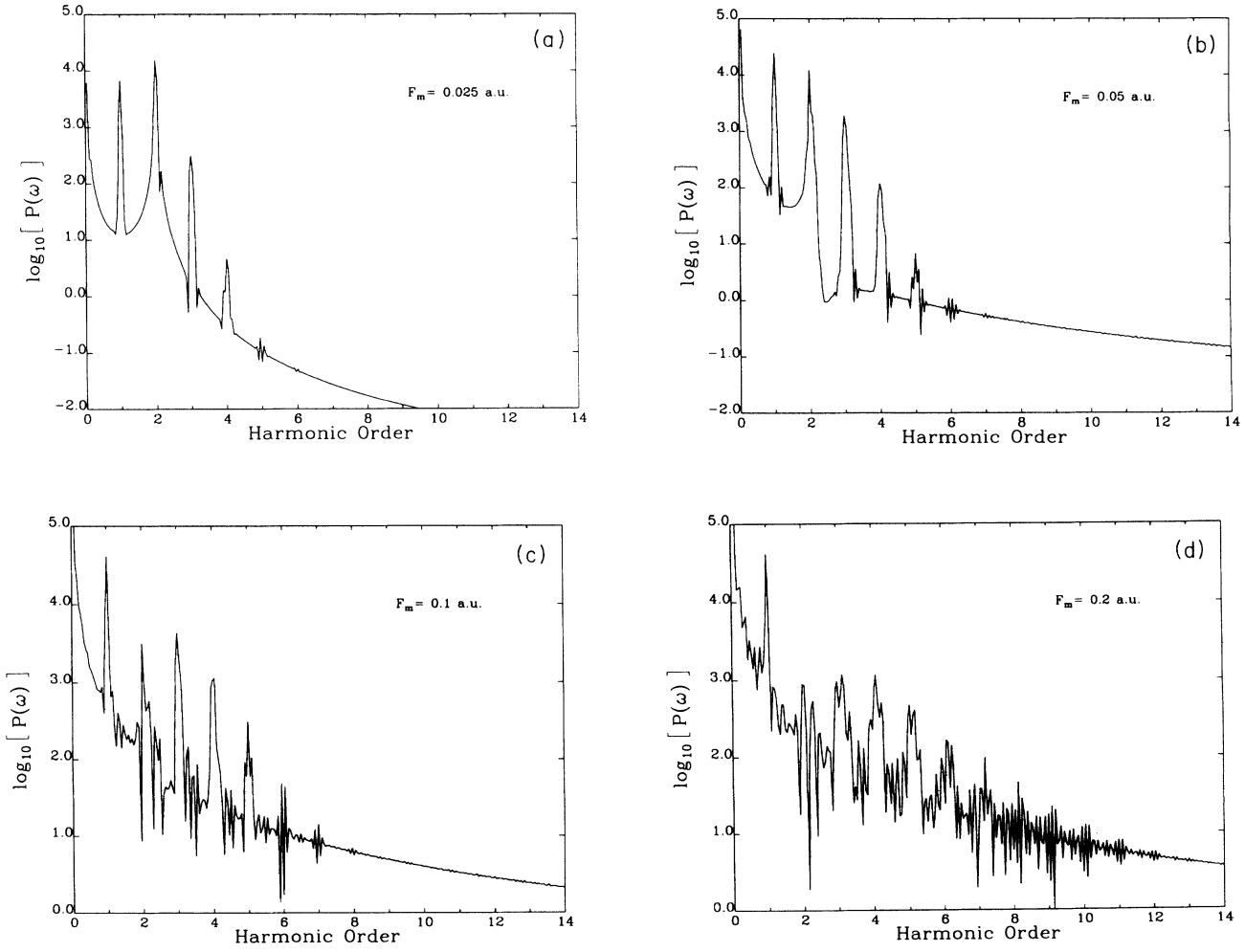

FIG. 4. Harmonic-generation spectra calculated from $\langle\ddot{x}(t)\rangle$. The horizontal axis is in units of photon energy. (a) F_m = 0.025 a.u., (b) F_m = 0.05 a.u., (c) F_m = 0.1 a.u., (d) F_m = 0.2 a.u.

survival populations are significant during the excitation process. However, the ATI peaks for the F_m =0.025 case are rather unpronounced, so we examine the case of F_m =0.05 a.u. In Fig. 7(b), we overlay the corresponding harmonic and ATI spectra for comparison. The harmonic spectrum is scaled onto the perpendicular axis for plotting convenience. The photon energies are above the threshold shift; the resemblance in structure is clear. The calculation supports the view of Eberly, Su, and Javanainen [21] on this point.

C. Numerical considerations

Most numerical schemes converge to the exact solutions for large N. The aim is to find a method that represents the physics accurately even for small N. If we are interested in the dynamics of continuum states of electrons, the p-space discretization provides a much more accurate approximation to the continuum energy eigenstates. We have shown that the ground state and several bound states are accurately represented, which permits us to capture effects that occur during the early stages of ionization. Admittedly the potential and dipole driving terms are not represented to a high accuracy for large x. But once the electron is ionized, the exact shape of the potential or the driving force may not matter as much, and we still capture the essential features of the dipole time dependency and the Coloumb well, such that the electron accurately continues to capture photons after ionization. The coincidence that the ground state has an extent comparable to the most ionized ATI regimes further encourages the study of strong-field problems in p space.

Some work remains to be done to optimize integration algorithms if two-dimensional simulations are to succeed. Because the Schrödinger equation is known to be numerically unconditionally unstable, simple leapfrog schemes will not work. The full Hamiltonian matrix makes semi-implicit integration costly, since a matrix inversion would have to be performed at every time step. But the potential gain from the increased understanding of strong-field processes sufficiently justifies further work at improving

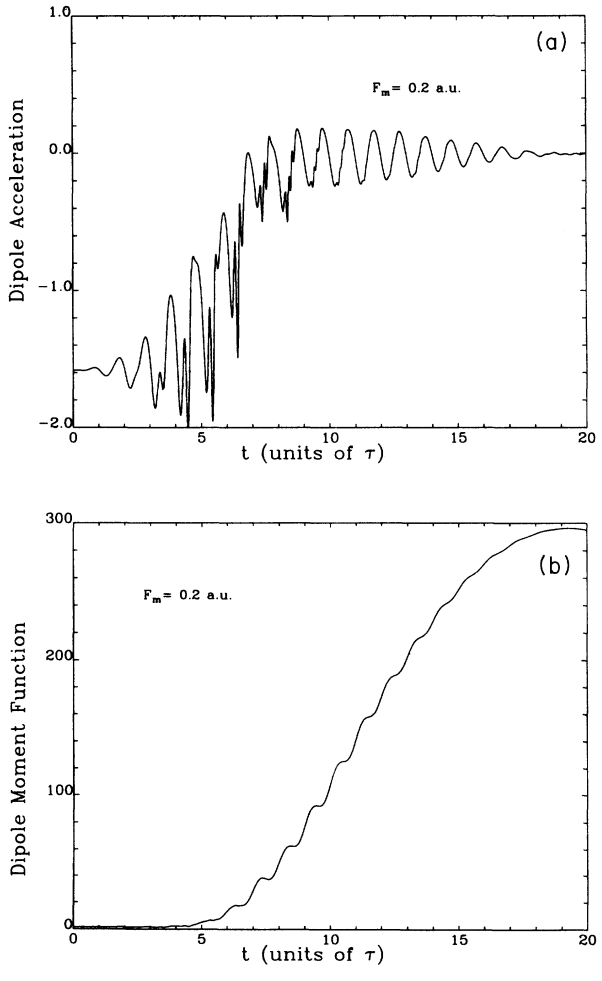

FIG. 5. (a) $\langle \ddot{x}(t) \rangle$ as a function of time. (b) $\langle x(t) \rangle$ as a function of time.

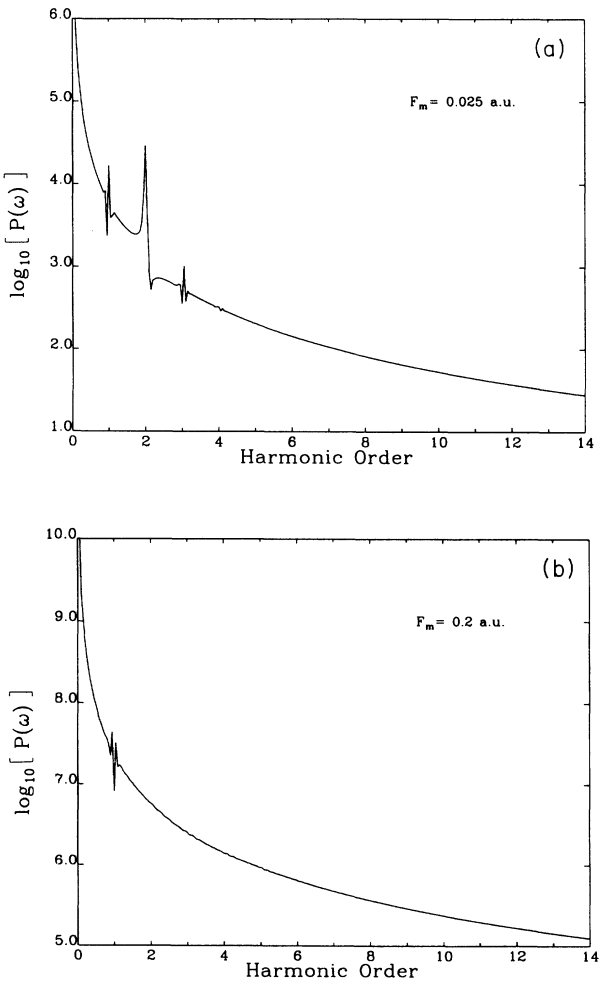

FIG. 6. Harmonic-generation spectra calculated from $\langle x(t) \rangle$. (a) $F_m = 0.025$ a.u., (b) $F_m = 0.2$ a.u.

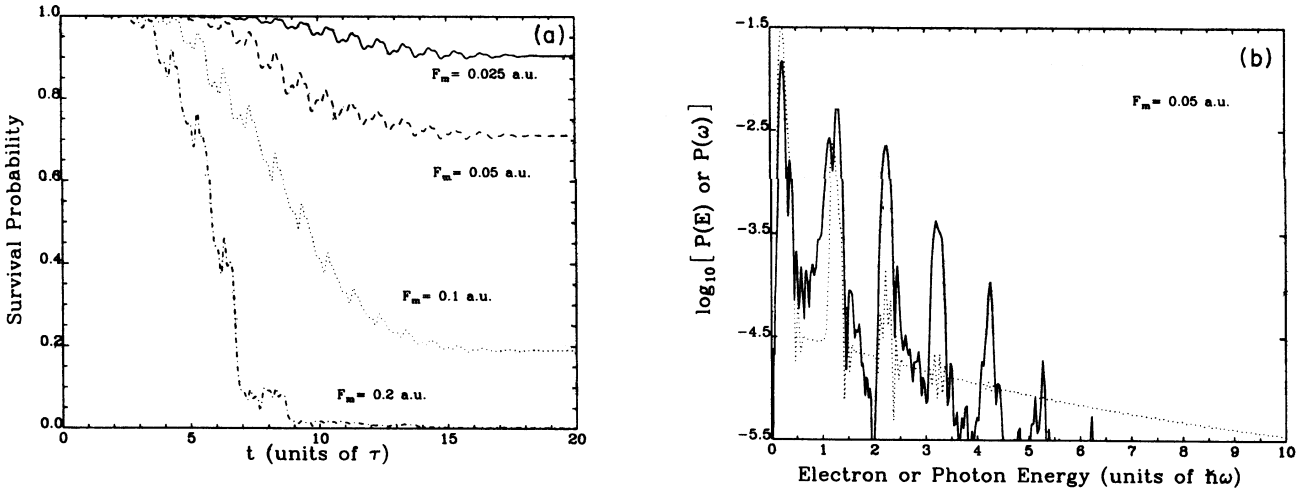

FIG. 7. (a) Survival probability of the ground state as a function of time for $F_m = 0.025$, 0.05, 0.1, and 0.2 a.u. (b) Comparison of the spectra shapes at $F_m = 0.05$ a.u., solid curve, ATI; dotted curve, harmonic generation with photon energy above the shifted threshold.

the current simple toy scheme, which already yields powerful results.

IV. CONCLUSION

In this paper we presented a direct p space method to study the ATI and harmonic-generation problems. The general features of ATI structure are well reproduced. Our other study [19] suggests that the angular momentum components are increasingly important in harmonic-generation processes at higher field strengths. The simulation of harmonic generation accentuates the need for the inclusion of angular momentum states. The one-dimensional model should be applied with caution to the harmonic-generation problem.

In the search of a more physical and predictive picture of strong-field continuum interactions, the p-space approach promises to shed more light on the physics of the underlying processes. It captures the ionized electron dynamics well, providing a valuable tool for numerically investigating time-dependent problems. The implementation of this method to ATI or harmonic-generation processes of real three-dimensional systems is currently under investigation to compare with the multiphoton experiments on a real hydrogen atom [15,22]. Studies on atomic stabilization in superintense fields and other interesting topics will be reported later.

ACKNOWLEDGMENTS

T.F.J. thanks Professor Der-San Chuu for many helpful comments and encouragement. Many stimulating communications with Professor Shih-I Chu are gratefully acknowledged. This work is supported by the National Science Council of Taiwan under Contract No. NSC-81-0208-M009-05. Support of the National Chiao Tung University through use of their Convex C-240 computer is also acknowledged.

* Present address: Department of Astrophysical Sciences, Princeton University, Princeton, NJ 08544-1001.

[1] P. Agostini, F. Fabre, G. Mainfray, G. Petite, and N. K. Rahman, Phys. Rev. Lett. **42**, 1127 (1979).

[2] For a recent review on experimental investigations, see, for example, R. P. Freeman and P. H. Bucksbaum, J. Phys. B **24**, 325 (1991); on theoretical aspects, see the thematic issue edited by K. Kulander and A. L'Huillier J. Opt. Soc. Am. B **7**, 407 (1990).

[3] Shih-I Chu and J. Cooper, Phys. Rev. A **32**, 2769 (1985); M. Dörr, R. M. Potvilege, and R. Shakeshaft, *ibid.* **41**, 558 (1990); X. Tang and S. Basile, *ibid.* **44**, 1454 (1991); M. Pont, D. Proulx, and R. Shakeshaft, *ibid.* **44**, 4486 (1991).

[4] J. Javanainen, J. H. Eberly, and Q. Su, Phys. Rev. A **38**, 3430 (1988); J. H. Eberly, Q. Su, and J. Javanainen, Phys. Rev. Lett. **62**, 881 (1989); Q. Su and J. H. Eberly, Phys. Rev. A **43**, 2474 (1991); **44**, 5997 (1991); V. C. Reed and K. Burnett, *ibid.* **42**, 3152 (1990); K. Burnett, P. L. Knight, B. R. M. Priaux, and V. C. Reed, Phys. Rev. Lett. **66**, 301 (1991); V. C. Reed, P. L. Knight, and K. Burnett, *ibid.* **67**, 1415 (1991); V. C. Reed and K. Burnett, Phys. Rev. A **43**, 6217 (1991); R. Grobe and C. K. Law, *ibid.* **44**, R4114 (1991).

[5] See, for example, Shih-I Chu and T. F. Jiang, Comput. Phys. Commun. **63**, 482 (1991).

[6] D. ter Haar ed., *Problems in Quantum Mechanics*, 3rd ed. (Routledge Chapman & Hall, New York, 1975, problem 3.43); the formula is $\frac{\hat{1}}{x} = -\frac{i}{\hbar}\int_{-\infty}^{p} f(p')dp'$.

[7] R. Loudon, Am. J. Phys. **27**, 649 (1959); L. K. Haines and D. H. Hoberts, *ibid.* **37**, 1145 (1969).

[8] J. G. Leopold and I. C. Percival, Phys. Rev. Lett. **41**, 944 (1978); D. Richards, J. Phys. B **20**, 2171 (1987); J. G. Leopold and D. Richards, *ibid.* **21**, 2179 (1988).

[9] R. V. Jensen, Phys. Rev. Lett. **49**, 1365 (1982); Phys. Rev. A **30**, 386 (1984).

[10] P. A. M. Dirac, Proc. R. Soc. London Ser. A **109**, 642

(1926).
[11] Ue-Li Pen and T. F. Jiang (unpublished).
[12] J. P. Keener, *Principles of Applied Mathematics* (Addison-Wesley, New York, 1988), p. 175.
[13] S. M. Susskind and R. V. Jensen, Phys. Rev. A **38**, 711 (1988).
[14] $p = 0.1$ is not one of our discrete continuum eigenvalues; the nearest value to $p = 0.1$ is the 33rd eigenstate for the parameters $p_{\max} = 5$, $N = 1000$ used in our calculations. The value of $p = 0.101\,26$ is used to compare with Ref. [13].
[15] G. A. Kyrala and T. D. Nichols, Phys. Rev. A **44**, 1450 (1991).
[16] S. M. Susskind and R. V. Jensen, Phys. Rev. A **38**, 711 (1988). For the three-dimensional hydrogen atom, see V. Fock, Z. Phys. **98**, 145 (1935).
[17] K. Burnett, V. C. Reed, J. Cooper, and P. L. Knight, Phys. Rev. A **45**, 3347 (1992).
[18] A. McPherson, G. Gibson, H. Jara, U. Johann, T. S.Luk, I. A. McIntyre, K. Boyer, and C. K. Rhodes, J. Opt. Soc. Am. B **4**, 595 (1987). See also, M. Ferray, A. L'Huillier, X. F. Li, L. A. Lompré, and G. Mainfray, J. Phys. B **21**, L31 (1988); X. F. Li, A. L'Huillier, M. Ferray, L. A. Lompré, and G. Mainfray, Phys. Rev. A **39**, 5751 (1989).
[19] Tsin-Fu Jiang and Shih-I Chu (unpublished).
[20] Shih-I Chu, K. Wang, and Eric Layton, J. Opt. Soc. Am. B **4**, 425 (1990), Ref. 24.
[21] J. H. Eberly, Q. Su, and J. Javanainen, Phys. Rev. Lett. **62**, 881 (1989).
[22] B. Wolff, H. Rottke, D. Feldmann, and K. H. Welge, Z. Phys. D **10**, 35 (1988); H. Rottke, B. Wolff, M. Brickwedde, D. Feldmann, and K. H. Welge, Phys. Rev. Lett. **64**, 404 (1990).